REPORT DOCUMENTATION PAGE

Form Approved
OMB No. 0704-0188

PLEASE DO NOT RETURN YOUR FORM TO THE ABOVE ADDRESS.

1. REPORT DATE *(DD-MM-YYYY)*	2. REPORT TYPE	3. DATES COVERED *(From - To)*
09/08/2009	Final	8/1/2006-8/31/2009

4. TITLE AND SUBTITLE

Tunnel Quantum Dot Intersubband Detector for Terahertz Frequencies

5a. CONTRACT NUMBER

5b. GRANT NUMBER

FA 9550-06-1-0500

5c. PROGRAM ELEMENT NUMBER

6. AUTHOR(S)

Professor Pallab Bhattacharya

5d. PROJECT NUMBER

5e. TASK NUMBER

5f. WORK UNIT NUMBER

7. PERFORMING ORGANIZATION NAME(S) AND ADDRESS(ES)

Professor Pallab Bhattacharya
Department of Electrical Engineering and Computer Science
University of Michigan, 1301 Beal Avenue
Ann Arbor, MI 48109-2122

8. PERFORMING ORGANIZATION REPORT NUMBER

UM 053314

9. SPONSORING/MONITORING AGENCY NAME(S) AND ADDRESS(ES)

Dr. Gernot S. Pomrenke, Program Manager
Physics and Electronics Directorate
Air Force Office of Scientific Research
875, N. Randolph Street
Arlington, VA 22203-1768

10. SPONSOR/MONITOR'S ACRONYM(S)

AFOSR

11. SPONSOR/MONITOR'S REPORT NUMBER(S)

12. DISTRIBUTION/AVAILABILITY STATEMENT

Approved for public release; distribution unlimited

13. SUPPLEMENTARY NOTES

The views, opinions and/or findings contained in this report are those of the author)s) and should not be construed as an official AFOSR position, policy or decision, unless so designated by other documentation

14. ABSTRACT

The most significant accomplishments in this project are: (a) the demonstration of a semiconductor based terahertz detector using quantum dots, capable of detection at high temperatures (80-150K) with very low dark currents: (b) a bias-selective multicolor long wavelength quantum dot intersublevel detector with tunability over 3 distinct wavelengths. The detector incorporates a novel double barrier tunneling heterostructure with each absorbing quantum dot layer; (c) a novel intersubband quantum ring terahertz detector with a resonant tunneling filter to reduce the dark current, hich is the lowest ever measured. This device demonstrates terahertz detection with 0.4A/W in the 3-6THz range and detection in the 10-11 ThZ range at 120K.

15. SUBJECT TERMS

terahertz detection, quantum dots, quantum rings

16. SECURITY CLASSIFICATION OF:			17. LIMITATION OF ABSTRACT	18. NUMBER OF PAGES	19a. NAME OF RESPONSIBLE PERSON
a. REPORT	b. ABSTRACT	c. THIS PAGE			Pallab Bhattacharya, EECS, U. of Michigan
unclassified	unclassified	unclassified	UL	12	19b. TELEPHONE NUMBER *(Include area code)* 734-763-6678

Reset

Standard Form 298 (Rev. 8/98)
Prescribed by ANSI Std. Z39.18

FINAL REPORT (UNABRIDGED VERSION)

To: technicalreports@afosr.af.mil and
Program Manager Dr. Gernot S. Pomrenke — gernot.pomrenke@afosr.af.mil

From: Professor Pallab Bhattacharya, University of Michigan, EECS/SSEL
Subject: FINAL REPORT (AFOSR FA9550-06-1-0500)
Date: August 31, 2009

Contract/Grant Title: Tunnel Quantum Dot Intersubband Detector for Terahertz Frequencies
Contract/Grant #: FA9550-06-1-0500
Reporting Period: 8/1/2006 to 9/30/2009
Personnel: Professor Pallab Bhattacharya,
Guan Huang,
Dr. Wei Guo,
Professor A.G.U. Perera, Georgia State University (Collaborator),
Dr. Gamini, Ariyawansa, Georgia State University (Collaborator).

Accomplishments:

Significant Accomplishments:
The most significant accomplishments in this project are: (a) the demonstration of a semiconductor based terahertz detector using quantum dots, capable of detection at high temperatures (80-150K) with very low dark currents: (b) a bias-selective multicolor long wavelength quantum dot intersublevel detector with tunability over 3 distinct wavelengths. The detector incorporates a novel double barrier tunneling heterostructure with each absorbing quantum dot layer; (c) a novel intersubband **quantum ring** terahertz detector with a resonant tunneling filter to reduce the dark current, which is the lowest ever measured. This device demonstrates terahertz detection with 0.4A/W in the 3-6THz range and detection in the 10-11 THz range at 120K. A more detailed description of these accomplishments follows.

1. High Temperature Multicolor Terahertz Quantum Dot Detectors

Our objective was to demonstrate a QDIP with a simple quantum dot heterostructure in the active region, having strong photoresponse at relatively high temperatures at the two wavelength ranges of interest. We have therefore designed the device with multiple layers of $In_{0.4}Ga_{0.6}As/GaAs$ quantum dots. An 8-band **k·p** model was used to calculate the dot electronic states with the effects of strain included with the valence force field model. The actual dot size is estimated from atomic force microscopy (AFM) measurements on a dot ensemble. The quantum dots grown by molecular beam epitaxy (MBE) typically have near-pyramidal shape with an average base width of 21nm and height of 5nm. The calculated energy levels in these dots are shown schematically in Fig. 1(a). Also shown in the figure are the wavelengths of photons that can be absorbed by the

dots due to intersublevel transitions, provided the initial states are filled with electrons. Thus radiation corresponding to wavelengths ~8μm, 18μm and 60μm are expected to be absorbed, based on the calculations.

The $In_{0.4}Ga_{0.6}As$/GaAs photoconductive QDIP heterostructure was grown by MBE on a (001)-oriented semi-insulating GaAs substrate. The active region consists of 20 $In_{0.4}Ga_{0.6}As$/GaAs quantum dots layers separated by 500 Å thick GaAs layers. The dots and spacers were grown continuously at 500°C. The quantum dots are n-doped with silicon with an estimated doping level of 1 electron per dot. This doping level is very critical since it is essential to have electrons in the initial states for the various transitions at different temperatures.

Devices for measurement are mounted on to chip carriers and gold wire contacts are made from individual devices to separate leads of the carrier. The chip carrier is mounted in a variable temperature cryostat (4.2 – 300 K) for dark current and spectral response measurements. The measured temperature-dependent dark current-voltage characteristics of a typical device of mesa diameter 600μm are shown in Fig. 1(b). The current densities at a bias of -2V are 2.55×10^{-6}, 5.58×10^{-2}, and 1.17A/cm^2 at 4.2, 80 and 140K, respectively. We attribute the relatively low dark current to three-dimensional confinement in the quantum dots, optimized doping of the dots and the presence of the GaAs barrier layers.

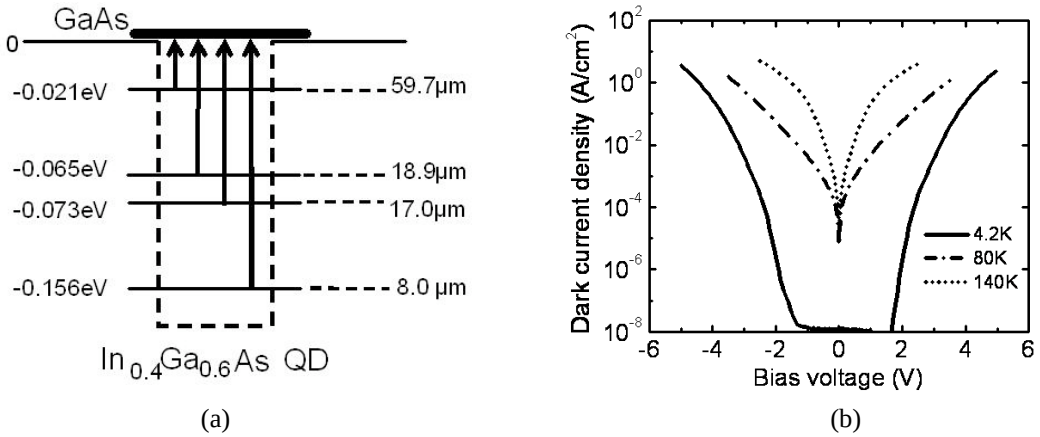

(a) (b)

Figure 1 (a) Electron energy levels in an $In_{0.4}Ga_{0.6}As$/GaAs self organized quantum dot calculated with an 8-band **k·p** model. The shape of the dot was assumed to be pyramidal with base 21nm and height 5nm; (b) measured temperature-dependent dark current voltage characteristics of a QDIP with 600μm diameter illumination area.

The calibrated spectral response of the QD photodetector at 80K and 120K with bias of -3V and -2V, respectively, is shown in Fig. 2(a). Two response peaks are observed in the range of 3-13μm and 20-55μm. The response in the 3-13μm range is centered at ~8μm and has peak responsivities of 0.86A/W and 0.19A/W at 80K and 120K, respectively. The response from 20-55μm is fairly broad with peak responsivities of 0.05A/W and 0.08A/W at 80K and 120K, respectively. The center of the peak is around 40μm. The sharp drop centered at ~36μm is due to longitudinal optical phonon absorption in GaAs, which has been reported in other experiments. Figure 2(b) shows the

measured and calibrated responsivity at 150K for an applied bias of -2V. The peak responsivity at ~40μm is still as high as 0.05A/W. These devices therefore offer the potential for high temperature terahertz detection.

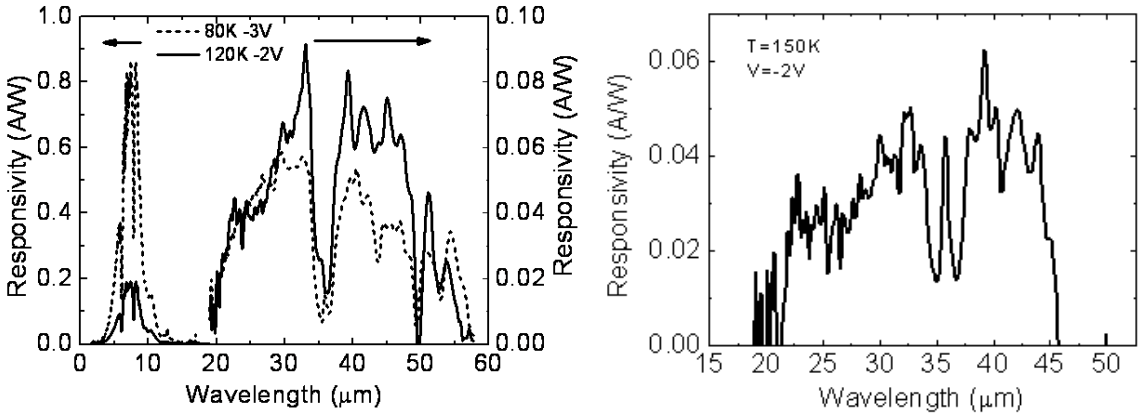

(a) (b)

Figure 2 Spectral responsivity of QDIPs measured at (a) 80K and 120K, and (b) 150K.

In comparing the measured spectral response with the calculated energies of the bound electron energy levels in the quantum dot, shown in Fig. 1(a), it is apparent that the response peaking at ~8μm corresponds to a transition of electrons from the ground state to the continuum. The response in the FIR region is believed to originate from transition of electrons from the dot excited states to the continuum. The reasons why the observed peak at ~40μm does not match exactly with the calculated excited states levels are: (a) the non-uniformity in the dot size broadens the response peaks; and (b) for 8 band **k·p** calculations, energy levels close to the band edge always have larger errors than levels far from the band edge. A shoulder to the FIR peak at ~22μm is distinctly seen in the data of Figs. 2(a) and (b) and this feature becomes more prominent at higher temperatures. Again, we believe, this peak result from transitions from the second excited states to the continuum.

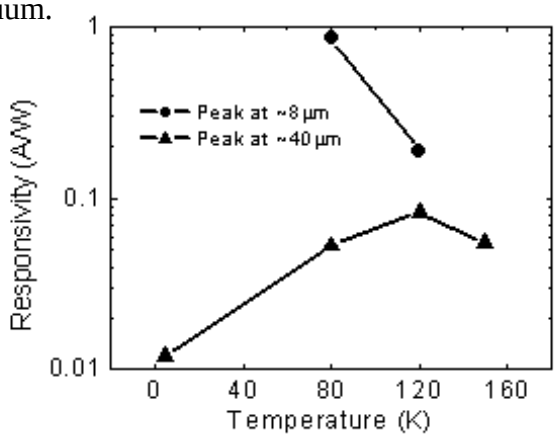

Figure 3 Variation of measured peak responsivity with temperature for absorption with peaks at 8μm and 40μm.

Further evidence of the origin of the peaks is provided by the temperature dependence of the peak responsivity, which is illustrated in Fig. 3. From 80 to 120K, the peak responsivity of the 8μm absorption peak decreases by ~80%, while the peak responsivity of the 40μm transition increases by a factor of 6 when the temperature increase from 4 to 120K. These trends can be accounted for by considering the thermal excitation of carriers from the ground state to excited states. Even the peak responsivity of the 22μm transition decreases from 0.04A/W to 0.03A/W, possibly due to thermal excitation from the second to higher excited states, as the temperature is increased from 120 to 150K.

The specific detectivity (D*), which is a measure of the signal-to-noise ratio of the device, was calculated from the measured peak responsivity R_p and noise density spectra S_i at different temperatures and applied biases. The noise spectra were measured with a dual channel Fast Fourier Transform (FFT) signal analyzer and a low noise pre-amplifier. A thick copper plate was used as a radiation block to provide the dark conditions for the measurements. The specific detectivity is calculated from $D^* = R_p A^{1/2} / S_i^{1/2}$. The values of D* for the 8μm peak are 2×10^9Jones at 80K (-3V bias) and 7.2×10^7Jones at 120K (-2V). For the 40μm peak the values of D* are 1.3×10^8Jones at 80K (-3V), 2.8×10^7Jones at 120K (-2V) and 2×10^7Jones at 150K (-2V). The D* value for the 8μm peak are lower than the best values that we and others have measured in the past and this is attributed to the higher dark current in these devices due to a higher doping level. However, the D* value for the terahertz absorption transition are larger than those reported earlier.

In conclusion, we demonstrate a multi-color QDIP with a simple quantum dot heterostructure absorption region. The device exhibits strong absorption peaks in the 3-13μm and 20-55μm ranges with large responsivity and detectivity at temperatures up to 150K.

2. Bias-selectable tricolor tunneling quantum dot intersublevel photodetector for atmospheric windows:

Multicolor infrared/THz detection has become an important tool in the field of IR/THz technology due to various applications. Detecting an object's IR/THz emission at multiple wavelengths can be used to eliminate background effects and reconstruct the object's absolute temperature. However, measuring multiple wavelength bands typically requires either multiple detectors or a single broadband detector with a filter wheel. These will require complicated detector assemblies, separate cooling systems, and numerous electronic and optical components. Consequently, such sensor systems (or imaging systems) require a complex control mechanism and hardware to achieve the fine optical alignment necessary, increasing the cost. These issues can be avoided by a single detector responding in multiple bands. Quantum dot-based detectors exhibit multi-color characteristics, which provides an ideal solution for multi-spectral detection. During the first year of the project, we have demonstrated a multi-color quantum dot intersublevel detector with photoresponse in the terahertz range (refer to accomplishment 1). However, the control or selection of these different response peaks for a single device becomes a key issue.

To solve this problem, we incorporated a novel two double-barrier (DB) system into a multicolor QD intersublevel photodetector and demonstrated the use of applied bias to

select the operating wavelength. The heterostrucure is designed such that an excited state in the QD coincides with a bound state in a DB system under certain bias conditions. The T-QDIP detector structure was grown by molecular beam epitaxy (MBE). The active region consists of pyramidal-shape $In_{0.4}Ga_{0.6}As$ QDs sandwiched between two DB systems that consist of an $In_{0.1}Ga_{0.9}As$ quantum well in 30 Å thick $Al_{0.2}Ga_{0.8}As$ barriers. The widths of the $In_{0.1}Ga_{0.9}As$ wells in bottom-DB (BDB) and top-DB (TDB) systems are 60 and 40 Å, respectively. There are ten periods of these QDs coupled with DBs and each period is separated with an undoped 400 Å thick GaAs layer. QDs with height and base dimensions of the ~6 and ~20 nm, respectively, are *n*-doped to $1\times10^{18}cm^{-3}$ using Si as the dopant, while all other layers are undoped except the GaAs bottom- and top-contact layers (*n*-doped to $2\times10^{18}cm^{-3}$). Vertical circular mesas for top illumination were fabricated by standard photolithography, wet chemical etching, and contact metallization techniques. The *n*-type top ring contact and the bottom contact were formed by evaporated Ni/Ge/Au/Ti/Au with thickness of 250/325/650/200/2000 Å. The radius of the optically active area of a processed device was 300 μ m. Devices for testing were mounted on to chip carriers with silver epoxy and gold wire contacts were made from the device to the chip carrier leads.

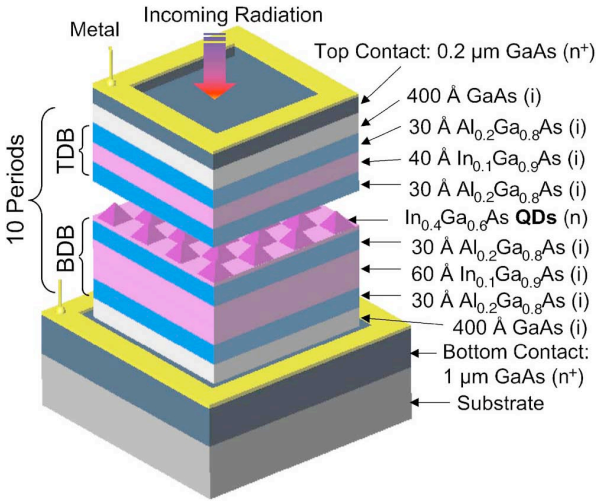

Figure 4 A 3D view of the processed T-QDIP structure grown by MBE. $In_{0.4}Ga_{0.6}As$ QDs are placed in between two DBs (top and bottom DBs indicated by TDB and BDB, respectively). The letter "i" indicates that the layer is intrinsic.

Photoabsorption takes place in $In_{0.4}Ga_{0.6}As$ quantum dots (QDs) and the excited electrons are collected by resonant tunneling across the double barrier coupled to the QDs. The field dependent tunneling for excited carriers in T-QDIP is used to select the operating wavelength. The measured and calibrated spectral response for forward and reverse bias at 50 K is shown in Fig. 5(a). Under forward bias (2 V), two peaks were observed at 4.5±0.05 and 9.5±0.05 μ m due to transitions from QD ground state to the wetting layer state and to the second QD excited state, respectively. Under reverse bias (−3.25 V), two peaks were observed at 4.9±0.05 and 16.9±0.1 μm due to transitions from QD ground state to the wetting layer state and to the first QD excited state, while the peak at 9.5 μm (observed for forward bias) is not apparent.

According to the variation of the peak response with applied bias shown in Fig. 5(b), it is clearly evident that there is a specific voltage at which the maximum response for each peaks can be obtained. The 9.5 μm peak exhibits its maximum responsivity (0.9 mA/W) at 2.5 V, while the 16.9 μm peak has a maximum responsivity of 3 mA/W at −3.25 V. According to theoretical calculation, the voltage at which the maximum peak response appears corresponds to the voltage required (±3–±3.5 V) to level the QD excited states and DB states. When the bias is increased in the reverse direction, only the first QD excited state approaches the state in the BDB, while the second QD excited state deviates. Hence, only the carriers excited to the first QD excited state will undergo resonant tunneling. At −3.25 V bias the 16.9 μm peak is very strong and the 9.5 μm peak is weaker by a factor of 50. However, when the forward bias is increased, both the first and second QD excited states approach the state in the TDB, opening resonant tunneling conditions for carriers excited into both QD states. Consequently, both 9.5 and 16.9 μm peaks are visible under forward bias and the 16.9 μm peak reaches its maximum response for a higher bias voltage than that for the 9.5 μm peak.

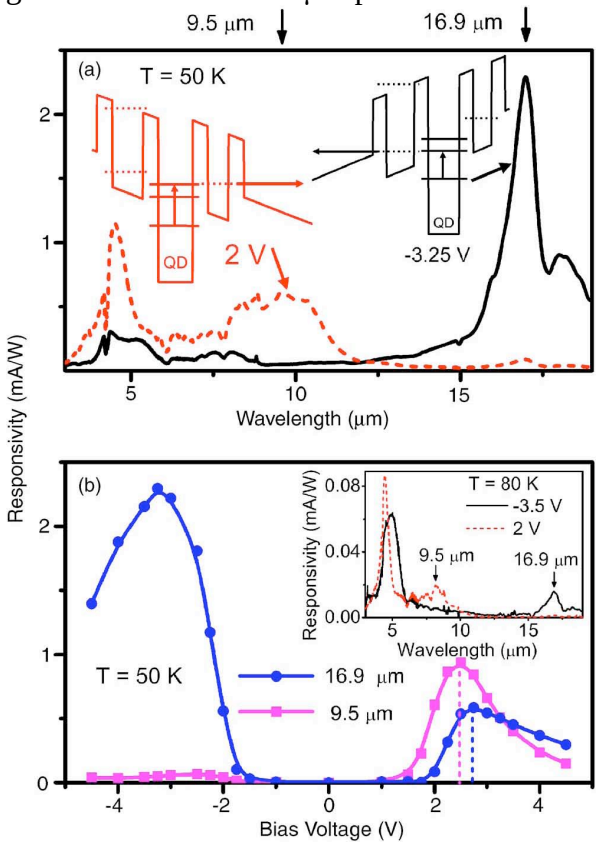

Figure 5 (a) Spectral responsivity of the T-QDIP detector at 50 K under 2 and −3.25 V bias. The energy state alignments under these bias conditions are also shown. (b) Variation of the peak responsivity with applied bias. By alternating the bias polarity, the detector can be operated at 9.5 or 16.9 μm.

The temperature dependence of the response showed that all the peaks with the peak selectivity can be observed up to 80 K [see Fig. 5(b)], while the short peak (4.5–5 μm) can be observed up to 100 K. The dark current densities at 80 and 300 K are ~4×10^{-8} A/cm^2 at ±4 V and ~8×10^{-4} A/cm^2 at ±2 V, respectively. This comparatively low dark

current is attributed to dark current blocking by the DBs. The detectivity values at 50 K for the peaks at 4.5(2 V), 9.5 (2 V), and 16.9 μm (−3.25 V) are 3.0, 1.6, and 6.0×10^{12} Jones, respectively.

In conclusion, a tricolor infrared detector with bias-selectable peaks based on tunneling quantum dot intersubband photodetector architecture is demonstrated. This T-QDIP exhibits three distinct response peaks at 4.5/ 4.9, 9.5, and 16.9 μm up to 80 K. Bias polarity allows the selection of either the 9.5 μm or the 16.9 μm peak.

3. Quantum ring terahertz detector with resonant tunnel barriers:

Quantum confinement based intersubband detectors utilizes transitions from excited states in the confined structures to continuum states in the bulk material for the absorption and detection of electromagnetic waves in the far infrared to terahertz range. Hence, the energy spacing ΔE between the two states determines the detection frequency. To extend the detection range into the 10-3THz region, it is intuitive to develop nanostructures with a smaller energy spacing ΔE. Smaller quantum dots have thus been experimented with in the past to achieve this goal. More recently, it is apparent that the quantum ring structure is a good candidate for this application since it demonstrates significant shift of electronic and hole energy states towards the barrier material bandedge, leading to smaller ΔE, compared to quantum dots. At the same time, since the rings are developed from quantum dots, the 3-D confinement of carriers is retained. The associated advantages include normal incidence response, low dark current, and high responsivity. These are essential for compact, high speed, and high sensitive terahertz detectors operating at high temperatures.

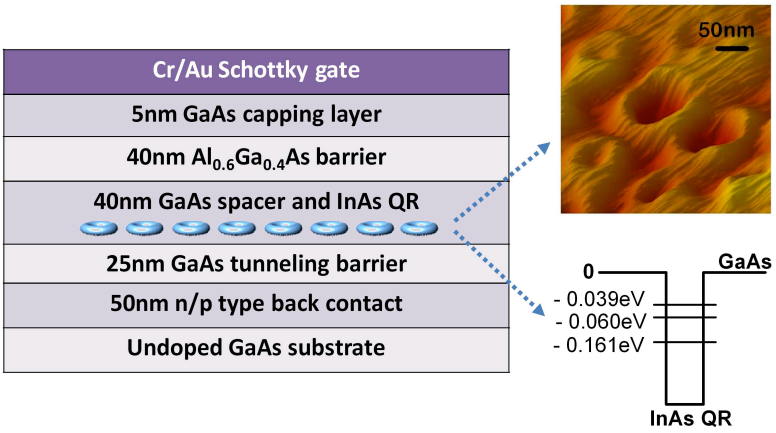

Figure 6 Schematic heterostructure of Schottky diode for capacitance-voltage measurements grown by MBE. Insets show AFM image of InAs quantum rings and calculated electron energy states.

The electron energy levels of the quantum rings were calculated by solving the time-independent Schrodinger equation within the effective mass approximation. The ring was modeled as a 2nm high hollow cylinder with inner and outer radius of 25nm and 40nm, respectively. The resulting eigenvalue problem is solved numerically and the calculated energy levels in the quantum ring are depicted in Fig. 6. Capacitance-voltage (C-V)

measurements were made at 10K to determine the spectral position of the bound electron and hole levels in the quantum rings. The device heterostructure grown by MBE is schematically shown in Fig. 6. The quantum rings are embedded in an undoped GaAs matrix and are formed as follows. After growth of the GaAs tunneling barrier layer at 600°C, the substrate temperature was lowered to 530°C and 2.6 monolayers of InAs was deposited at a rate of 0.05 monolayer/sec. Self-organized quantum dots were formed following growth of 1.8 monolayers of an InAs wetting layer. A 10Å/10Å GaAs/AlAs cap layer was grown on the InAs islands at 530°C. Growth was interrupted and the capped islands were annealed at 560°C for 1 min, under an As_2 flux to form the quantum rings. Atomic force microscopy (AFM) imaging of exposed QR layers (Fig. 6) indicates that the aerial density of the rings is ~$10^{10}cm^{-2}$. The rest of the heterostructure, starting with the 40nm undoped GaAs spacer layer, was grown at a substrate temperature of 600°C. Two heterostructures were grown, with n- and p-type back contact layers, for the measurement of electron and hole energy levels, respectively. Diode structures having 640μm diameter mesas with Cr/Au Schottky gates on top and appropriate alloyed back contacts were fabricated by standard optical lithography, wet etching and metallization techniques. By changing the dc bias, the equilibrium Fermi level can be moved in energy inside the GaAs band gap and through all electron and hole quantized levels in the quantum rings. The measured capacitance is the sum of the geometric capacitance (inversely related to the sample thickness), the density-of-states capacitance, and a capacitance resulting form charge accumulation in different parts of the heterostructure. The measured C-V characteristics for the n- and p-type samples are shown in Fig. 7. The plateaus in the two cases correspond to carrier accumulation in the 2-D wetting layer, while the peaks labeled E_{ground} and H_{ground} are believed to originate from the electron and hole ground states of the quantum ring. The calculated excited states of the quantum rings are not observed. From analysis of the measured data, the confinement energy of the electron and hole ground states, with respect to the GaAs band edges, are estimated to be 150meV and 98meV, respectively. The former is in reasonably good agreement with the calculated value, quoted earlier.

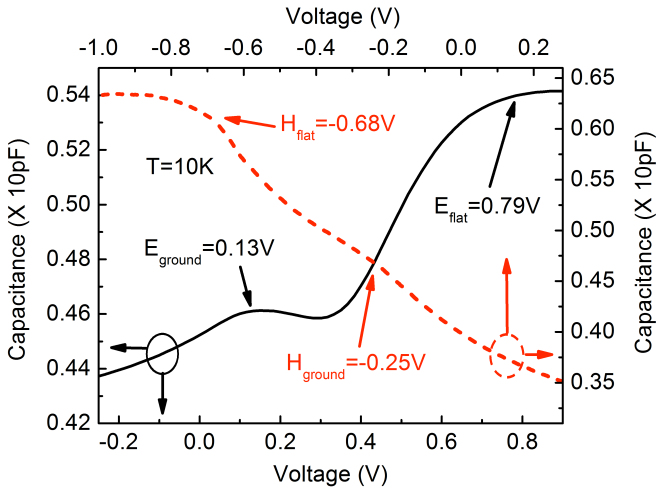

Figure 7 Capacitance-voltage measurement data from quantum ring heterostructures. The electron and hole ground state energies obtained from the analysis of these data are in good agreement with calculated values.

A critical parameter in the operation of long-wavelength detectors is the dark current, which should be as small as possible to enhance the specific detectivity D*. The conduction band profile of one period of the quantum ring with the resonant tunneling structure and the complete heterostructure with 15 quantum ring layers (to enhance absorption) and grown by MBE are shown in Fig. 8(a). The double-barrier resonant tunneling heterostructure preferably transports the photoexcited electrons, while blocking a significant fraction of the electrons (with an energy spread) that contribute to the dark

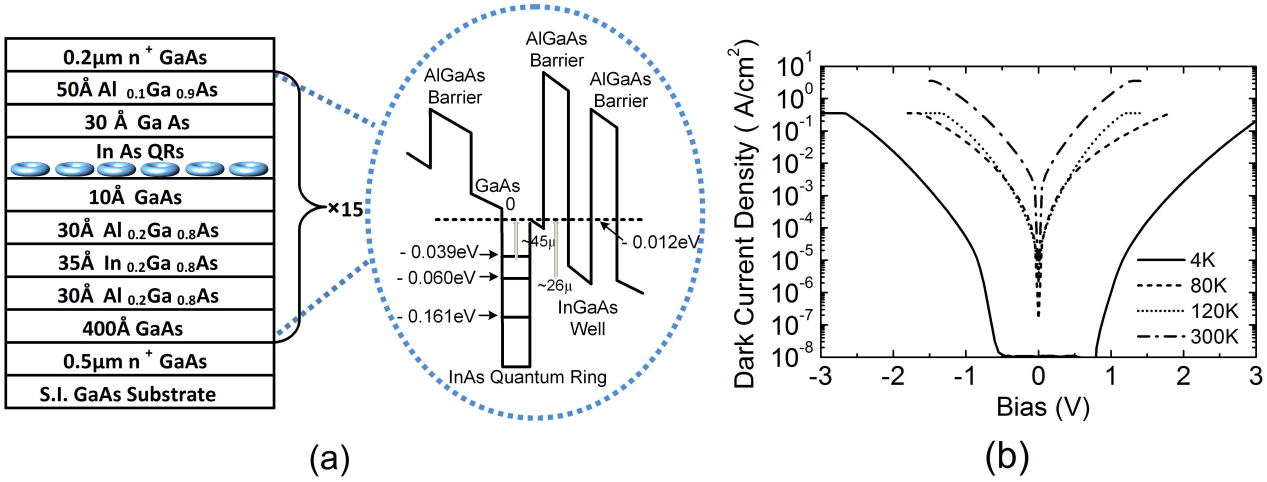

Figure 8 (a) Heterostructure schematic of QRID grown by MBE. The inset depicts one period of the quantum ring layer together with double barrier resonant tunneling heterostructure; (b) Measured temperature-dependent dark current as a function of bias.

current. The calculated electron energy levels in the quantum ring are also indicated in the figure. The energy levels in the quantum well are calculated by solving the one-dimensional Schrödinger equation including the presence of the wetting layer. Tunability in the energy position of these energy levels is afforded by varying the height (composition) of the single AlGaAs barrier. Mesa-shaped devices for top illumination were fabricated by photolithography, wet chemical etching and n-contact metallization. The ring-shaped top contact has an inner radius of 300 µm, which defines the illumination area.

The dark current-voltage characteristics in the temperature range of 4-300K are shown in Fig. 8 (b). The dark currents are comparable to and low as those measured in previously reported resonant tunneling QDIPs. The current densities at a bias of -1V are 5×10^{-5}, 4.7×10^{-2} and 3.5×10^{-1}A/cm^2 at 4.2, 80 and 300K, respectively. The normal incidence spectral response was measured with a globar broadband source and a System 2000 Perkin Elmer Fourier transform infrared (FTIR) spectrometer. For this study we have focused in the spectral range of 20-100 µm (3-15THz). The calibrated spectral response of the QRID devices at 5, 80 and 120K with an applied bias of -2V, are shown in Fig. 9. It is apparent that the data indicate three responsivity peaks at ~6.5 THz (46µm), 10THz (30µm) and 12.5THz (24µm). The longitudinal optical phonon absorption in GaAs and AlAs are seen as the resonances (dips) at ~8.3 THz(36 µm) and 11THz (27

μm), respectively. The peaks at 48 μm and 25 μm correspond extremely well with transitions originating from the two calculated QR excited states, shown in Fig. 8(a), to the quantum well/ resonant tunneling state. The origin of the responsivity peak centered at 30 μm is not well understood at this time. One possibility is the existence of additional confined states, due to the non-trivial geometry of the quantum rings, which are not determined from the simple effective mass calculation. It may also be noted that the 46μm transition is not observed in the 120K measurement data, but the transitions at 24 and 30μm are still present. In general, the transitions appear to be broad because they are

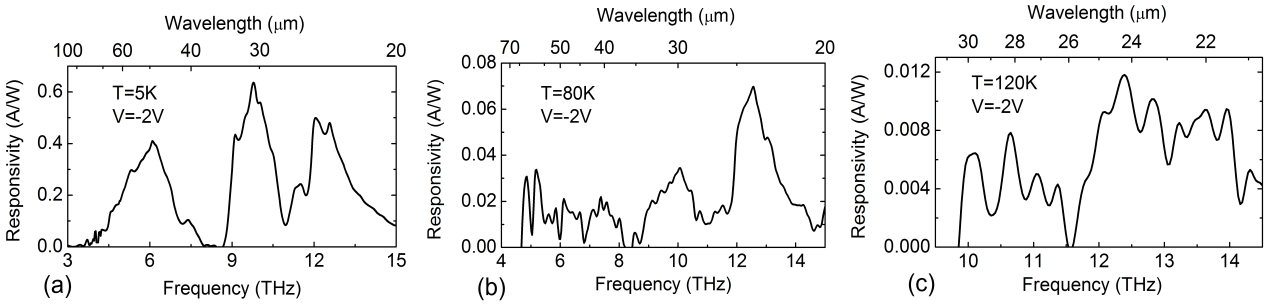

Figure 9 Calibrated spectral responsivity of resonant tunneling quantum ring intersubband detectors measured at (a) 5K, (b) 80K, and (c) 120K.

at very long wavelengths. The width of the 46μm peak at 5K is only 7.5meV. It is of interest to note that at 5K, the peak responsivities corresponding to the three transitions are almost comparable though they are widely separated in wavelength. At 80K, the peak amplitude decreases with increasing wavelength. At 120K, the peak amplitudes of both observable transitions are weak. Generally, the peak responsivity in the THz range shows a decreasing trend with increasing temperature. There are two competing factors that determine the relative magnitude of the temperature dependent responsivity of the different absorption peaks. For the same incident power, there are more photons at longer wavelengths. Also, with increase of temperature, the occupation of the higher excited states decreases by thermionic emission. Finally, the noise performance becomes a significant factor, although our tunnel filter helps to a large extent.

The QRID noise current was measured with a current pre-amplifier and Fast Fourier Transform signal analyzer. A thick copper plate was used to shield the device from outer radiation. The specific detectivity (D*), a measure of the signal-to-noise ratio of the THz detector was calculated from the noise density spectra and responsivity in accordance with the relation $D^* = R_p A^{1/2} / S_i^{1/2}$, where A is the illumination area and S_i is the noise density spectra. The values of D* for the 10THz response peak at 5 and 80K are 4.9×10^9 Jones and 9.5×10^7 Jones, respectively, at a bias of -2V.

Conclusion:

Novel long-wavelength and terahertz detectors have been designed and fabricated and their detection characteristics have been measured as a function of temperature. Three classes of novel devices have been demonstrated and investigated. The first is a

multi-frequency quantum dot terahertz detector which demonstrates large responsivity upto 45 μm at a temperature as high as 150 K. The second device is a quantum dot intersublevel detector with double resonant tunneling filters. The device demonstrates good bias tunability of detection at 4.5, 9.5, and 16.5 μm. The third is a terahertz detector with quantum rings as the absorption media. The electronic properties and quantum states of the rings have been calculated and measured using the capacitance-voltage technique. Three responsivity peaks at 6.5, 10.0, and 12.5 THz are measured at temperatures of 80 and 120 K. The dark current of these devices are ~10^{-1} A/cm^2 at 300 K, the lowest recorded for a terahertz detection devices. These devices promise to become a serious contender for high-temperature terahertz detection.

Doctoral Dissertation:

Guan Huang: Multicolor quantum dot/ring intersublevel detector for infrared and terahertz detections

Date of defense: November 2, 2009

Archival publications (published) during reporting period:

1. "Room Temperature Nano and Micro Structure Photon Detectors", A.G.U. Perera, P.V.V. Jayaweera, G. Ariyawansa, S.G. Matsik, K. Tennakone, M. Buchanan, H.C. Liu, X.H. Su and P. Bhattacharya, *Microelectronics Journal* **40**, 507 (2009).

2. "A quantum ring terahertz detector with resonant tunnel barriers", G. Huang, W. Guo, P. Bhattacharya, G. Ariyawansa, and A. G. U. Perera, *Appl. Phys. Lett.* **94**, 101115 (2009).

3. "Wavelength agile superlattice quantum dot infrared photodetector", G. Ariyawansa, A. G. U. Perera, G. Huang, and P. Bhattacharya, *Appl. Phys. Lett.* **94**, 131109 (2009).

4. "Bias-selectable tri-color tunneling quantum dot infrared photodetector for atmospheric windows", G. Ariyawansa, V. Apalkov, A. G. U. Perera, S. G. Matsik, G. Huang, and P. Bhattacharya, *Appl. Phys. Lett.* **92**, 111104 (2008).

5. "A Multi-Color Quantum Dot Intersublevel Detector with Photoresponse in the Terahertz Range", G. Huang, J. Yang and P. Bhattacharya, G. Ariyawansa and A. G. U. Perera, *Appl. Phys. Lett.* **92**, 011117, (2008).

6. "High-Temperature Tunneling Quantum-Dot Intersublevel Detectors for Mid-Infrared to Terahertz Frequencies", P. Bhattacharya, Xiaohua Su, G. Ariyawansa, A. G. U. Perera, *Proceedings of the IEEE* **95**, 1828– 1837 (2007).

Conference Presentations:

1. "Properties of InAs/GaAs Quantum Rings and Their Application to Terahertz Detection", G. Huang, W. Guo, P. Bhattacharya, G. Ariyawansa, A. G. U. Perera, *EMC 2009*, University Park, PA, June 24-26, 2009.

2. "Bias Selectable Dual-Band Quantum Dot Infrared Detectors" A.G.U Perera, G. Ariyawansa, G. Huang, and P. Bhattacharya, *International Conference on Quantum Structure Infrared Photodetectors*, Yosemite, CA, January 2009.

3. "Tunneling Quantum Dot Sensors for Multi-Band Infrared and Terahertz Radiation Detection", G. Ariyawansa, S. Matsik, V. Apalkov, A. G. U. Perera, X. Su, and P. Bhattacharya, *IEEE Sensors 2007*, Atlanta, GA, October 2007.

Awards and honors during reporting period:

1. Professor P. Bhattacharya was elected member of the National Academy of Engineering.
2. Professor P. Bhattacharya received the 2007 IEEE Nanotechnology Pioneer Award.
3. Professor P. Bhattacharya received the 2008 TMS John Bardeen Award.